Pressure Transient Analysis of Naturally Fractured Reservoirs with Uniform Fracture Distribution

H. KAZEMI*
JUNIOR MEMBER AIME

ATLANTIC RICHFIELD CO.
DALLAS, TEX.

ABSTRACT

An ideal theoretical model of a naturally fractured reservoir with a uniform fracture distribution, motivated by an earlier model by Warren and Root, has been developed. This model consists of a finite circular reservoir with a centrally located well and two distinct porous regions, referred to as matrix and fracture, respectively. The matrix has high storage, but low flow capacity; the fracture has low storage, but high flow capacity. The flow in the entire reservoir is unsteady state.

The results of this study are compared with the results of the earlier models, and it has been concluded that major conclusions of Warren and Root are quite substantial. Furthermore, an attempt has been made to study critically other analytical methods reported in the literature.

In general, it may be concluded that the analysis of a naturally fractured reservoir from pressure transient data relies considerably on the degree and the type of heterogeneity of the system; the testing procedure and test facilities are sometimes as important. Nevertheless, under favorable conditions, one should be able to calculate in-situ characteristics of the matrix-fracture system, such as pore-volume ratio, over-all capacity of the formation, total storage capacity of the porous matrix, and some measure of matrix permeability.

INTRODUCTION

The analysis of flow and buildup tests for obtaining in-situ characteristics of oil and gas reservoirs has received considerable attention in the past decade.

Most of the available techniques result in reliable conclusions in macroscopically homogeneous reservoirs or in the homogeneous reservoirs with only certain types of induced and/or inherent heterogeneity (such as wellbore damage, etc.). In general, the greater the degree of heterogeneity, the less the reliability of the information deduced from the pressure transient data. A commonly encountered heterogeneous system is a naturally fractured reservoir where two types of distinct porosities occur in the same formation. The region containing finer pores may have high storage and low flow capacities. This is called the matrix. The remaining region may have high flow capacity with low storage. The latter region is generally the set of interconnecting fractures and fissures of the rock, and for this reason it is called the fracture. Ordinarily, we wish to obtain the permeability and porosity of each region and perhaps the frequency of the fracture distribution in a reservoir. Such information is necessary for reservoir engineering. Other information, such as wellbore damage, will be useful in evaluating possible remedial work for such fields. Few authors have suggested theories to aid in calculating the in-situ characteristics of a naturally fractured reservoir similar to what we have described above. Pollard[1] suggested that a naturally fractured reservoir contained three distinct regions: a damaged or an improved region surrounding the wellbore, and the two remaining regions the same as described earlier. He suggested that the flow was taking place from the tight matrix into the highly conductive fractures, then into the wellbore region and finally into the well column. He concluded that the average pressure buildup in each of these distinct regions can be expressed approximately in terms of an exponential decay function of time. He also hypothesized that the decay coefficients for each of these functions were significantly different from each other; consequently, each of these functions became dominant in turn, in the process of pressure buildup. Thus, by a proper graphic plot of the logarithm of wellbore pressure differences vs buildup time, each of these functions could be determined (see Fig. 1). Pollard suggested methods of determining the wellbore damage and fracture volume. Later Pirson and Pirson[2] extended

Original manuscript received in Society of Petroleum Engineers office July 8, 1968. Revised manuscript received June 23, 1969. Paper (SPE 2156A) was presented at 43rd Annual Fall Meeting held in Houston, Tex., Sept. 29-Oct. 2, 1968.

*Presently associated with Marathon Oil Co., Littleton, Colo.

This paper will be printed in *Transactions* volume 246, which will cover 1969.

[1]References given at end of paper.

Pollard's method to calculate matrix volume as well.

The graphic method of Pollard and formulas of Pirson-Pirson for interpretation of the wellbore pressure data have had apparent success; however, it was shown by Warren and Root[3] that such results obtained from a synthesized homogeneous infinite formation were considerably in error. We will also show, by our model, that such errors prevail for a finite fractured reservoir.

Warren and Root used a different approach to study naturally fractured reservoirs. They assumed that a reservoir can be represented by a set of building blocks (parallelepipeds) where the blocks represented the matrix and the spacing between the fractures. They also assumed that formation fluid flows into the fractures and the high conductivity fractures carry the fluid to the wellbore column. In this process, it was assumed that the flow in the fracture was unsteady state, while in the matrix it was quasi-steady state. They concluded that the pressure buildup curve (as plotted in the conventional manner) would have two parallel straight-line sections whose slopes were related to the flow capacity of the formation; the vertical separation of the two lines was related to the relative storage capacity of the fracture (see Fig. 2). There are a number of points in favor of Warren and Root's model. For instance, they have evidenced field cases where the buildup plot resembles the theoretical plot convincingly.[4]

Odeh[5] represented a model quite similar to that of Warren and Root and concluded that a fractured reservoir buildup curve behaves like the buildup curve of a homogeneous reservoir. This, of course, contradicted the results of Warren and Root. However, it can be shown that, if the building block dimensions are small (e.g., 3 ft) and the matrix permeability high (e.g., greater than 0.01 md), his conclusions are valid for all practical purposes. In support of Warren and Root's model, it is interesting to know that, for instance, in the fractured reservoirs of Southwestern Iran, the matrix permeability is in the range of 0.00005 to 0.5 md and the fracture blocks are huge.[14]

A recent paper by Pickett and Reynolds[6] reports on the experiments they have conducted on a highly fractured formation in a pre-Cambrian gneiss with no matrix porosity. They concluded that the Pollard graphic method fits the data extremely well. They did not report on any calculations based on the graphic parameters suggested by Pollard or Pirson.

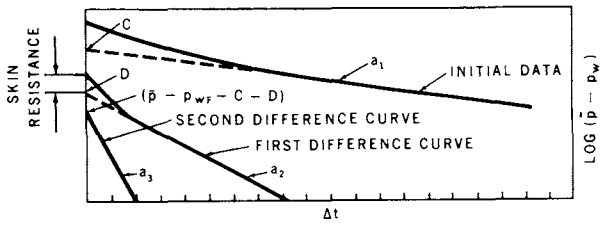

FIG. 1 — POLLARD PLOT OF PRESSURE BUILDUP DATA. (AFTER PIRSON AND PIRSON[2])

We feel that the curve obtained by Pickett and Reynolds could be an indication of what is known as "late transient" portion of pressure fall-off curve (see Matthews and Russell[7]), for which the graphic representation is identical.

In the preceding papers oil was the dominant flowing phase. A case of gas flow in a vugular, dolomitic fractured reservoir was presented by Adams *et al.*,[10] where the gas was fairly dry. They noticed that some of the preceding models could explain the pressure buildup curves of numerous wells in this field. Actually, they observed two slopes where the first one had a higher value than the second slope. The conclusion was that the first slope would yield matrix permeability and the second one would yield the mean permeability of the fracture-matrix system. We feel that in the absence of other possibilities such an explanation is plausible, and a paper by Huskey and Crawford,[11] which studies the effect of nonconnecting vertical fractures on over-all flow behavior, could shed additional light on the subject.

Other papers have been written on multiphase flow in vugular fractured reservoirs; however, in these papers only the long-term reservoir engineering aspects of flow have been emphasized and none could have been applied to pressure buildup tests.

Let us, for a moment, go back to a curve obtained by Warren and Root. As it is shown in Appendix B, the minimum time required for a typical building block of their model to reach quasi-steady state is about the same as the time where the first straight line should disappear. At first sight this implies that in a realistic situation, the first straight line may not develop as such. If so, a vital piece of information, the relative storage capacity of the fracture, may no longer be calculable. Therefore, to ensure the validity of this apparent weakness of Warren and Root's model and perhaps other hidden inconsistencies, we chose a simplified version of their model reservoir and removed the restriction of quasi-steady state from the matrix, replacing it by unsteady state. We concluded that the pressure buildup curve, based on this model, resembled

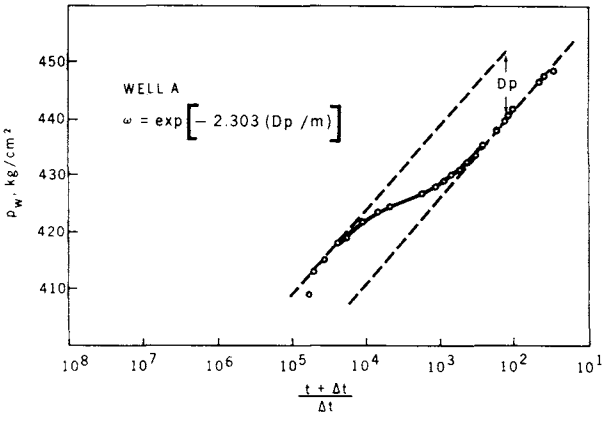

FIG. 2 — FIELD BUILDUP CURVE. (AFTER WARREN AND ROOT[4])

Warren and Root's and, furthermore, that some of their quantitative findings were accurate. Other conclusions inferred from the shape of the buildup curves will appear later in the report.

THEORY

A special case of the idealized fractured reservoir of Warren and Root[3] is adopted for this work. This special case can be thought of in two different ways. First, it is one in which all the fractures are horizontal (see Fig. 3 and compare Idealization III with both II and I). Secondly, it is one in which all the fractures are replaced by an equivalent set of horizontal fractures. We chose horizontal fractures so that the equivalent flow in the fractures becomes radial and converging toward the wellbore. In either case, our idealized reservoir consists of a set of uniformly spaced horizontal matrix layers with the set of fractures as the spacers. If a well penetrates the formation, then the formation fluid enters the wellbore largely through the high flow capacity fractures. Since the matrix flow capacity relative to that of the fracture is extremely low, it can be assumed that flow enters the wellbore only at the penetrated fractures. Indeed, the soundness of this assumption was substantiated by allowing the whole sand face to flow (see Fig. 6).

A representative section of the model reservoir is shown by Fig. 4. The general assumptions governing this model follow.

1. There is single-phase flow.
2. The matrix with high storage and extremely low flow capacity produces into the fracture, which has low storage and high flow capacity. The fracture, in turn, produces into the wellbore.
3. Flow occurs in both radial and vertical directions.
4. Flow is unsteady state.
5. The reservoir is horizontal and the matrix and the fracture are each homogeneous and isotropic.
6. The well is centrally located in a finite circular reservoir.

The flow is described as follows.

$$\frac{1}{r}\frac{\partial}{\partial r}\left(r\frac{\partial \Phi}{\partial r}\right)+\frac{\partial^2 \Phi}{\partial z^2}=\frac{\phi_m \mu c_m}{k_m}\frac{\partial \Phi}{\partial t}\ ;$$

$$\frac{\delta}{2}<z<\frac{h}{2}\ ,\ r_w<r<r_e \quad \ldots\ (1)$$

$$\frac{1}{r}\frac{\partial}{\partial r}\left(k_f\, r\frac{\partial \Phi}{\partial r}\right)+\frac{k_m}{\delta/2}\left(\frac{\partial \Phi}{\partial z}\right)_{z=\delta^+/2}=$$

$$\phi_f \mu c_f \frac{\partial \Phi}{\partial t}\ ,\ 0<z<\frac{\delta}{2}\ ,\ r_w<r<r_e \quad (2)$$

$$\frac{\partial \Phi}{\partial r}=0\ ;\ \frac{\delta}{2}<z<\frac{h}{2}\ ,\ r=r_w$$

$$\text{and}\quad r=r_e \quad \ldots\ (3)$$

$$\frac{\partial \Phi}{\partial r}=-\frac{\mu B}{\pi k_f \delta r_w}\ q\ ;\ 0<z<\frac{\delta}{2}\ ,\ r=r_w \quad (4)$$

$$\frac{\partial \Phi}{\partial z}=0\ ;\ r_w<r<r_e\ ,\ z=0 \text{ and } z=\frac{h}{2} \quad \ldots\ (5)$$

$$\Phi\ (r,z,0)=\Phi_i \quad \ldots\ (6)$$

where

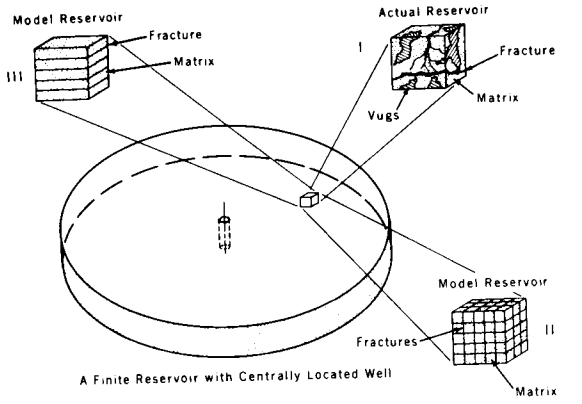

FIG. 3 — IDEALIZATION OF A NATURALLY FRACTURED HETEROGENEOUS POROUS MEDIUM. (II, WARREN-ROOT MODEL,[3] III, KAZEMI MODEL)

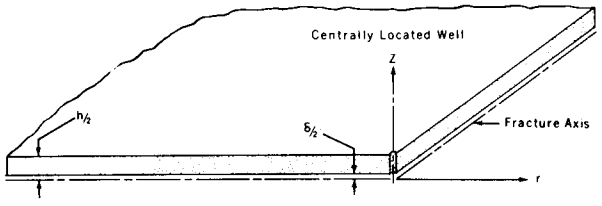

FIG. 4—REPRESENTATIVE SECTION OF THE MODEL RESERVOIR.

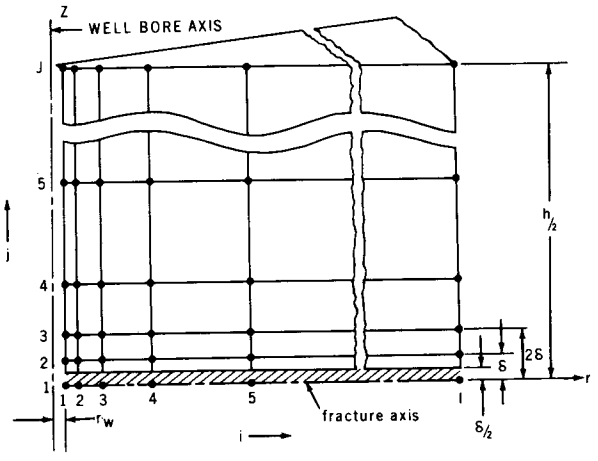

FIG. 5—GRID OF MESH POINTS FOR ADI PROCEDURE.

$$\Phi = \rho(0)\left[\int_0^p \frac{dp}{\rho(p)} + gz\right] \quad \ldots\ldots \quad (7)$$

Eqs. 1 and 2 are valid provided the fluid compressibility (about 10^{-5} psi^{-1}) and the spatial gradients of Φ are small. This particular representation of flow equation in terms of Φ is physically more meaningful, because for a slightly compressible fluid the instantaneous value of the potential Φ in the wellbore is constant, while the pressure varies from the top to the bottom of the sand. Nonetheless, for simplicity we replaced potential by the pressure p since the major conclusions will not alter for most of the practical cases.

The solution of Systems 1 through 6 was obtained by an iterative alternating direction implicit (ADI) procedure similar to the method of Ref. 8 (see Appendix C).

RESULTS

Three hypothetical cases, with properties appearing in Table 1, were synthesized. A typical pressure drawdown and a buildup are reported in Figs. 6 and 7. It can be observed from the large time portion of Fig. 6 that the boundary effect has not been sensed at the wellbore, while in Fig. 7 this effect is almost noticeable. Figs. 8 and 9 are the pressure buildup and drawdown of Case 2 where the boundary effect is noticeable. Fig. 10 is the pressure drawdown for Case 3, where again the boundary effect has begun. Fig. 11 is the replot of the quasi-steady state portion of the drawdown curve of Case 2 (see Fig. 8). The Pollard plots for Cases 1 and 2 are shown in Figs. 12 and 13, respectively. Notice that the data for preparation of these figures (Table 2) are taken from Figs. 7 and 9, respectively; they are located between the two straight-line segments and these segments correspond to early buildup data.

TABLE 1 — THE SYNTHESIZED SYSTEMS

Parameters	Case 1	Case 2	Case 3
ϕ_m	.05	.05	.08
ϕ_f	.45	1.00	.45
$h/2$	9.05	9.05	4.90
$\delta/2$	.025	.025	.025
k_m	.01	.01	1.0
k_f	7236.39	18098.00	5521.0
c_m	10^{-5}	6.0×10^{-6}	10^{-5}
c_f	10^{-5}	6.0×10^{-6}	10^{-5}
p_i	4000.0	3000.0	5000.0
q	90.5	90.5	200.0
μ	1.0	1.0	0.235
B	1.0	1.0	1.0
r_e	5280.0	2640.0	5280.0
r_w	0.375	0.375	0.375
Calculated according to Appendix D:			
c_1	10^{-5}	6.0×10^{-6}	10^{-5}
c_2	10^{-5}	6.0×10^{-6}	10^{-5}
ϕ_1	0.049862	0.049862	0.079592
ϕ_2	0.0012431	0.0027624	0.0022959
ω	0.024324	0.052493	0.028037
λ	2.576×10^{-6}	1.03×10^{-6}	6.025×10^{-4}
$\bar{k}$	20.0	50.0	29.163
$\bar{\phi}$	0.051105	0.052624	0.081888

ANALYSIS OF THE RESULTS

Figs. 6 through 10 indicate that both the pressure drawdown and the pressure buildup curves based on our model have two distinct slopes. This was the same conclusion reported by Warren and Root.[3] Nevertheless, a careful examination of the cases reported indicates that the results are not identical. It also appears that the previous theories can be critically reviewed. Incidentally, we have chosen to use the interpretative formulas of Warren and Root as a basis for our quantitative interpretations. The reliability of such equations is discussed in

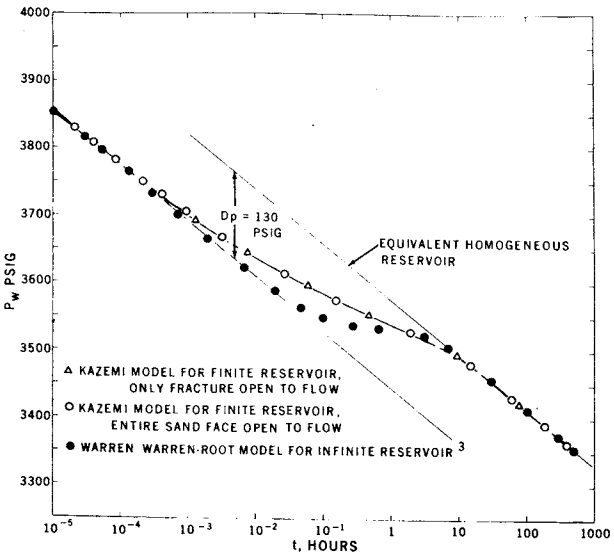

FIG. 6 — PRESSURE DRAWDOWN FOR CASE 1.

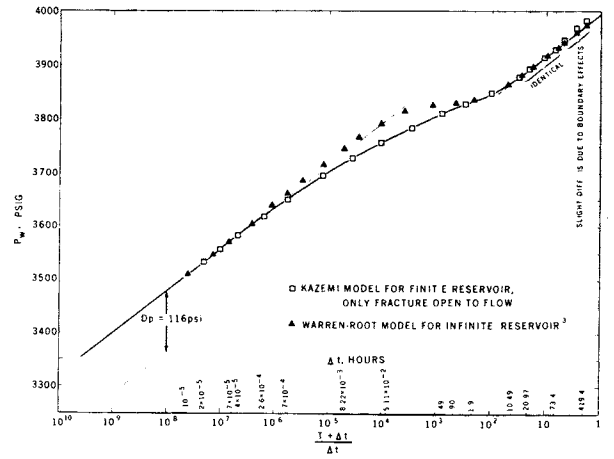

FIG. 7 — PRESSURE BUILDUP FOR CASE 1.

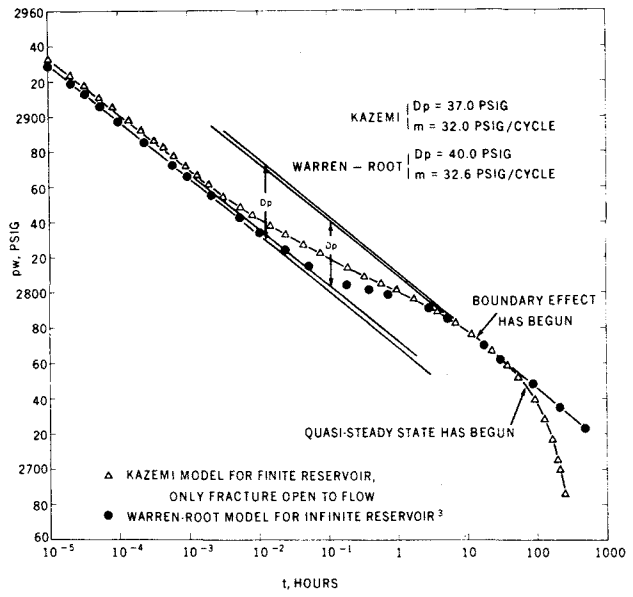

FIG. 8 — PRESSURE DRAWDOWN FOR CASE 2.

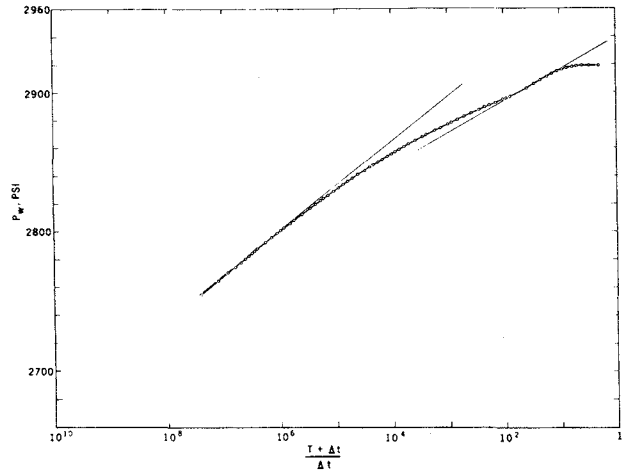

FIG. 9 — PRESSURE BUILDUP FOR CASE 2.

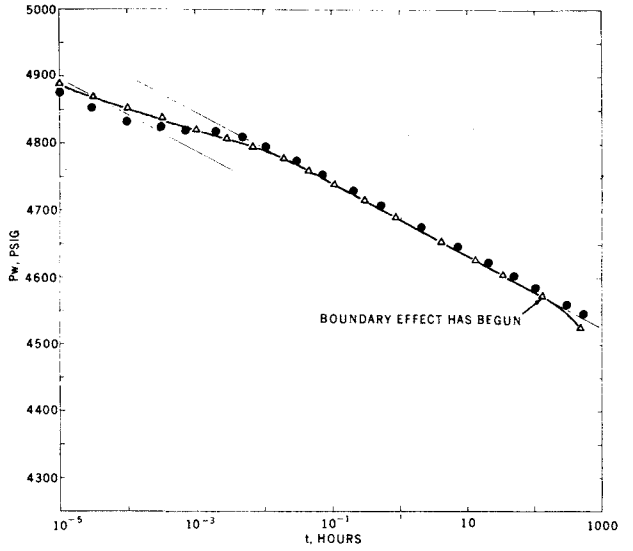

FIG. 10 — PRESSURE DRAWDOWN OF CASE 3.

the following paragraphs. The major equations are in Appendix B.

1. Fig. 6 indicates that if the boundary effect has not been sensed at the wellbore, if the matrix flow capacity is much smaller than the fracture flow capacity (such that $\lambda < 5 \times 10^{-6}$) and if the two parallel line segments of the drawdown curve have sufficient vertical separations, the slope m and the separation Dp yield accurate total flow capacity kh and storage capacity ratio ω. But from a practical point of view, a drawdown test of this nature is unlikely, because no practical drawdown

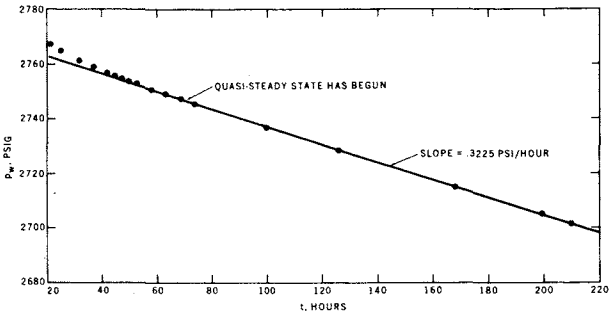

FIG. 11 — QUASI-STEADY STATE FOR CASE 2.

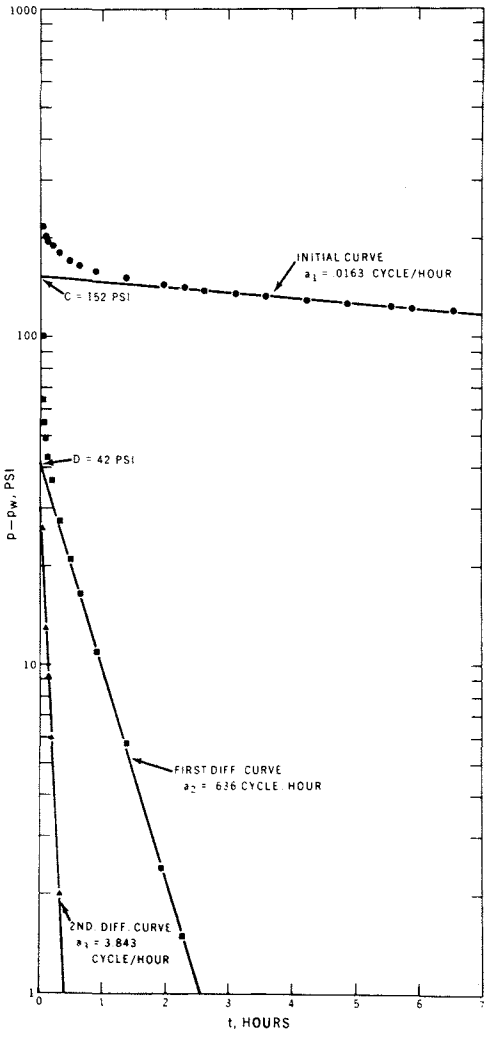

FIG. 12 — POLLARD PLOT OF CASE 1.

test can be initiated whose flow rate remains constant from the onset of the test. And since the first straight-line segment begins and terminates at very short times, the theoretical drawdown curves may be used only to study the basic differences of the models under investigation. For instance, the major difference between Warren and Root's model and ours is that we have replaced the condition of quasi-steady state flow in the matrix by unsteady state. Now, we try to delineate the differences. Referring to Fig. 6, it may be noticed that the pressure drawdown of Warren and Root and that of this study have two important differences. First, our early straight line is much shorter, and once flow reaches quasi-steady state conditions, the two plots converge more closely. Secondly, it is at early times only that our pressure levels are slightly higher than that predicted by Warren and Root. This is physically rational because our drawdown begins totally as an unsteady-state regime, and the average pressure before reaching quasi-steady state is higher.

2. More realistic than a drawdown test is a pressure buildup test, because the theory and practice are more compatible, especially in high potential liquid wells where they can be shut in with short after-flow duration. Further, bottom-hole shut-in is possible. Now, referring to Fig. 7, it may be noticed that the results of this study and those of Warren and Root are in very close agreement. In fact, the effective value of flow capacity may be calculated very accurately, while the value of ω is overestimated. The error depends highly on Dp, m and Dp/m. For instance, a large value of Dp (≥ 100 psi) introduces negligible errors; while, for $Dp < 100$, the error can be substantial.

3. The case of a finite reservoir where the boundary effects have substantially been sensed at the wellbore is shown by Figs. 8 and 9. If we consider only the buildup curve, we notice that because of the boundary effect, the second straight line is not parallel to the first. Thus, ω *cannot* be calculated. However, the first straight line yields correct value of the effective flow capacity, while the second one overestimates the value. Therefore, a word of caution is necessary, because in most practical cases most of the early straight lines are obscured by afterflow, damage, or nonavailability of the data. The use of the second straight line, then, would result in overestimating the flow capacity. Fig. 9 may be compared with Fig. 10.18 of Ref. 7, where it will be noticed that the two figures have good resemblance. This may also enable one to justify the proper straight-line section of a buildup curve in naturally fractured reservoirs.

4. Fig. 10 is the pressure drawdown of a case where λ is much larger than 5×10^{-6}. In this instance, the early straight line has formed in such a short time that its measurement is nearly impossible. The pressure buildup of the same well will also have a similar character. Thus, for a fractured reservoir of this nature, the pressure buildup curve will display only the second straight line, which, incidentally, substantiates the views of Odeh.[5]

5. Fig. 11 is a replot of the quasi-steady state portion of the drawdown curve for Case 1. Using the slope of the straight-line section and Eq. 10.14

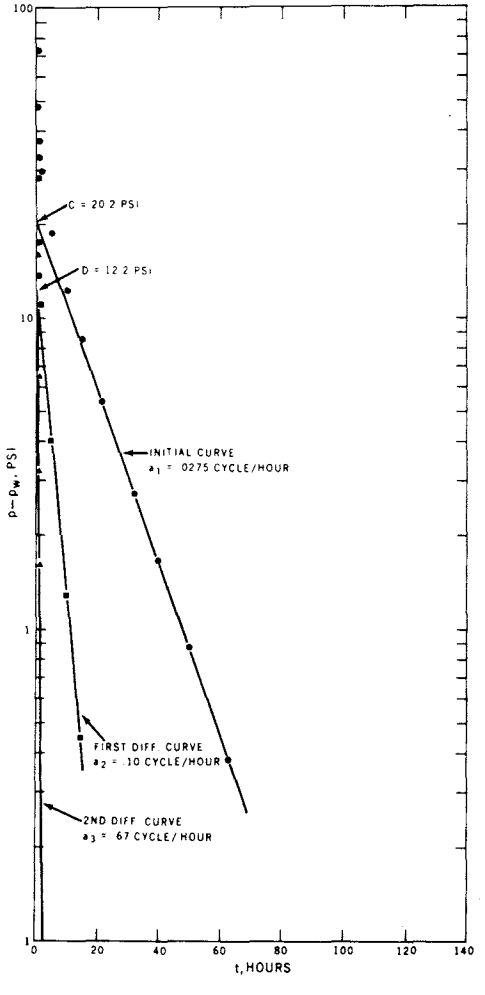

FIG. 13 — POLLARD PLOT OF CASE 2.

TABLE 2 — DATA FOR FIG. 12

Δt, hr	p_w, psi	$\bar{p}-p_w$, psi	Δp, psi	Δpp, psi	Summary of Calculations and Pertinent Data
0.0511	3763.00	215.97	64.0	26.0	$\bar{p}$ = 3987.97 psi
0.0767	3771.58	207.39	55.0	18.0	C = 152 psi
0.1023	3777.59	201.38	49.0	13.0	D = 43 psi
0.1432	3784.41	194.56	43.0	9.3	$\alpha_1 = 0.0163\ hr^{-1}$
0.2047	3791.56	187.41	36.4	6.0	$\alpha_2 = 0.636\ hr^{-1}$
0.3276	3800.71	178.26	27.5	2.0	$\alpha_3 = 3.843\ hr^{-1}$
0.4914	3808.50	170.47	21.0		$(PV_m)_{calc} = 2.9 \times 10^5$ cu ft
0.6543	3813.98	164.99	16.5		$(PV_f)_{calc} = 3.37 \times 10^4$ cu ft
0.9010	3820.00	158.97	11.0		$(PV_m)_{act} = 3.95 \times 10^7$ cu ft
1.393	3828.14	150.83	5.8		$(PV_f)_{act} = 9.85 \times 10^5$ cu ft
1.966	3834.57	144.40	2.4		E_f = −96.6 percent
2.290	3837.45	141.52	1.5		E_m = −99.5 percent
2.620	3839.98	138.99	0.0		
3.113	3843.27	135.70			
4.256	3849.43	129.54			
5.570	3855.08	123.89			
8.520	3865.16	113.81			
10.486	3870.70	108.27			
12.452	3875.61	103.36			

reported by Matthews and Russell,[7]

$$r_e^2 = 0.07455 \frac{qB}{\frac{dp}{dt} c_T (\phi h)_T} \quad \ldots\ldots (8)$$

one finds that only 2 percent error was introduced in the calculation of the reservoir radius. This indicates that behavior of a fractured reservoir, as described by our model, is nearly identical with the behavior of multilayer reservoir with crossflow. In fact, the quasi-steady state occurs at a time given by Eq. 9.

$$t = 1{,}580 \frac{(\phi h)_T u c_T r_e^2}{\bar{k}h_T} \text{ (hours)} \quad \ldots\ldots (9)$$

which is comparable to Eq. 10.13 of Ref. 7.

6. Figs. 12 and 13 are the Pollard[1] plots of Cases 1 and 2 (for times located between the two straight-line segments), respectively. It may be noticed that seemingly valid curves are obtained; however, there is considerable error in the pore volume calculations of matrix and fracture based on these plots and through the application of Eqs. A-2 and A-3, which were suggested by Pirson and Pirson. (Results are summarized in Table 2). This is an indication that the Pollard plot may have only an apparent validity.

7. By curiosity, we removed the restriction that the flow into the wellbore was only at the fracture openings; that is, we also allowed the matrix to flow into the wellbore. The result is shown in Fig. 6. Very little difference may be noticed. Hence, the quantitative conclusions are not affected.

8. The interference drawdowns affecting the observation wells, which were 662, 1,003 and 1,519 ft from the test well, are shown in Table 3. These drawdowns are the calculated values at the fracture level in the observation wells. The corresponding calculations for the equivalent homogeneous system are also shown. It may be noticed that the pressure drops at the observation wells are considerably higher for the fractured reservoir than for the equivalent homogeneous system. The pressure drops equalize at large times. This implies that the early interference results cannot be interpreted by conventional methods; however, at large times (provided the boundary effects are still negligible) the conventional interference analysis will result in calculation of total storage capacity, $(\phi_1 c_1 + \phi_2 c_2)h$. This knowledge, in addition to ω, should result in evaluating fracture-matrix pore ratio and calculation of interporosity flow parameter λ, as discussed in the Application section. The analytical solution to the interference problem in a naturally fractured reservoir and further results will appear in a later report.[15]

APPLICATION

From the aforementioned results one may conclude that in case of a large contrast in matrix-fracture flow capacities, the two-line buildup curve, as suggested by Warren and Root, will form. Indeed this materializes when interporosity flow parameter λ is very small (say, less than 10^{-6}). From such a curve one may calculate total flow capacity $\bar{k}h$ and pore storage ratio ω. Also, from an interference test the total storage capacity, $(\phi_1 c_1 + \phi_2 c_2)h$, may be obtained. Knowing the last three groups of parameters, $\phi_2 c_2$ and λ may be calculated. $\phi_2 c_2$ is calculated from ω and $(\phi_1 c_1 + \phi_2 c_2)h$, while λ is obtained from Eq. B-2, by assuming various values of λ until a match is obtained between field data and calculated points according to Eq. B-2. It is possible to match only the later straight-line section accurately.

Once $\phi_2 c_2$ and $\phi_1 c_1 + \phi_2 c_2$ are obtained, ϕ_1 and ϕ_2 may be roughly calculated. Also, using Eq. D-3, one may be able to calculate matrix permeability.

$$k_m = \frac{\bar{k}h^2}{12 r_w^2} \lambda \quad \ldots\ldots (10)$$

where $\bar{k}h$, r_w and λ are known. Notice that

$$\bar{k}h = \bar{k}h_T / N \quad \ldots\ldots (11)$$

CONCLUSIONS

This study concludes that:

1. The fractured reservoir characterizations of Warren-Root[3] are applicable to the cases where the fracture distribution is uniform and the contrast between fracture and matrix flow capacities is large. Thus, from a buildup test, the total flow capacity and ratio of storage capacities in such double porosity systems should be obtainable.

2. Combining the results of an interference test and a buildup test on the same well should yield an approximate value for matrix permeability.

3. Whenever the ratio of flow capacities in the matrix and in the fracture is small, only one straight line is noticeable, and this is in

TABLE 3 — INTERFERENCE PRESSURE DRAWDOWNS, PSI, FOR CASE I

	Well No. 1 at 661.9 ft		Well No. 2 at 1002.6 ft		Well No. 3 at 1518.8 ft	
t, hours	Fracture Model $i = 19$	Equivalent Model*	Fracture Model $i = 20$	Equivalent Model	Fracture Model $i = 21$	Equivalent Model
0.2866	0.243	0.000	0.013	0.000	0.000	0.000
0.4505	0.514	0.000	0.037	0.000	0.001	0.000
0.5733	0.735	0.000	0.062	0.000	0.002	0.000
0.7372	1.035	0.000	0.101	0.000	0.004	0.000
0.9830	1.484	0.000	0.169	0.000	0.009	0.000
1.311	2.064	0.001	0.273	0.000	0.016	0.000
1.966	3.137	0.025	0.504	0.000	0.038	0.000
3.277	4.998	0.341	1.001	0.003	0.099	0.000
4.915	6.980	1.39	1.637	0.043	0.198	0.000
7.864	10.126	4.43	2.803	0.407	0.421	0.004
10.49	12.734	7.59	3.882	1.11	0.663	0.028
15.73	17.657	13.8	6.159	3.29	1.263	0.230
19.66	21.115	18.2	7.931	5.26	1.803	0.563
31.46	30.322	29.0	13.277	11.5	3.766	2.36
47.19	40.346	39.8	19.997	19.1	6.838	5.73
68.16	50.815	50.6	27.853	27.5	11.165	10.6

*Equivalent model means an equivalent homogeneous model representing the naturally fractured system.

accordance with Odeh's[5] conclusions.

4. Pollard's plot of pressure buildup seems to have only an apparent validity in evaluating fracture-matrix pore volumes.

5. The behavior of a fractured reservoir approaches that of an equivalent system of homogeneous reservoir at large times.

NOMENCLATURE

a_1 = exponential decay coefficient for matrix, cycle/hour
a_2 = exponential decay coefficient for fracture, cycle/hour
a_3 = exponential decay coefficient for wellbore region, cycle/hour
B = oil formation volume factor, dimensionless
c = compressibility, (atm^{-1}) psi^{-1}
C, D = intercepts in Pollard's plot, psi
Dp = vertical separation of the buildup curve, psi
E = error, percent
g = gravity, (cm/sq sec) ft/sq sec
h = fracture block thickness, (cm) ft
h_T = reservoir thickness, (cm) ft
k = permeability, (darcy) md
$\bar{k}$ = average (or total) weighted radial permeability, md
m = drawdown or buildup slope, psi/cycle
N = number of fracture openings in wellbore
p = pressure, (atm) psi
$\bar{p}$ = equilibrium reservoir pressure, psi
p_w = well pressure, psi
p_{wf} = flowing well pressure, psi
PV = pore volume
q = flow rate, (cc/sec) STB/D
r = radial coordinate, (cm) ft
r_e = reservoir radius, (cm) ft
r_w = well radius (cm) ft
s = skin factor, dimensionless
t = flow time, (sec) hour
t_D = dimensionless time
t_D^* = time when first straight line disappears
T_D = total flow time, dimensionless
z = vertical coordinate, (cm) ft
δ = fracture thickness, (cm) ft
λ = interporosity flow parameter
μ = viscosity, cp
ρ = density, (gm/cc) slug/cu ft
ϕ = porosity, fraction
$\bar{\phi}$ = average bulk porosity
Φ = flow potential, (atm) psi*
ω = ratio of storage capacity of the fracture to total storage capacity
Δp = first difference for Pollard plot, psi
Δpp = second difference for Pollard plot, psi
Δt = buildup time, (sec) hour

SUBSCRIPTS AND SUPERSCRIPTS

1 = matrix; attached to bulk matrix properties
2 = fracture; attached to bulk fracture properties
f = fracture; attached to point fracture properties
i = radial mesh points
j = vertical mesh points
(k) = iteration number
m = matrix; attached to point matrix properties
n = time step
s = damaged zone
T = total (over-all) property

*Major equations are derived using Darcy units shown in parenthesis.

ACKNOWLEDGMENT

The cooperation of Sinclair Mediterranean Oil Co. is gratefully acknowledged.

REFERENCES

1. Pollard, P.: "Evaluation of Acid Treatments from Pressure Build-Up Analysis", *Trans.*, AIME (1959) Vol. 216, 38-43.
2. Pirson, R. S. and Pirson, S. J.: "An Extension of the Pollard Analysis Method of Well Pressure Build-Up and Drawdown Tests", Paper No. SPE 101 presented at the 36th Annual SPE Fall Meeting, Dallas, Tex., Oct. 8-11, 1961.
3. Warren, J. E. and Root, P. J.: "The Behavior of Naturally Fractured Reservoirs", *Soc. Pet. Eng. J.* (Sept., 1963) 245-255.
4. Warren, J. E. and Root, P. J.: "Discussion on Ref. 3 and Ref. 5", *Soc. Pet. Eng. J.* (March, 1965) 64-65.
5. Odeh, A. S.: "Unsteady-State Behavior of Naturally Fractured Reservoirs", *Soc. Pet. Eng. J.* (March, 1965) 60-66.
6. Pickett, G. R. and Reynolds, E. B.: "Evaluation of Fractured Reservoirs", *Soc. Pet. Eng. J.* (March, 1969) 28-38.
7. Matthews, C. S. and Russell, D. G.: *Pressure Buildup and Flow Tests in Wells*, Monograph Series, SPE of AIME, Dallas, Tex. (1967) Vol. 1, 50 and 73.
8. Vacher, J. P. and Cazabat, V.: "Ecoulement des Fluides dans les Milieux Poreux Stratifies. Resultats Obtenus sur le Modele du Biocouche avec Communication", *Revue IFP* (Oct., 1961) No. 10.
9. Peaceman, D. W. and Rachford, H. H., Jr.: "The Numerical Solution of Parabolic and Elliptic Differential Equations", *J. Soc. Indust. Appl. Math.* (March, 1955) Vol. 3, No. 1.
10. Adams, A. R., Ramey, H. J., Jr. and Burgess, R. J.: "Gas Well Testing in a Fractured Carbonate Reservoir", *J. Pet. Tech.* (Oct., 1968) 1187-1194.
11. Huskey, W. L. and Crawford, P. B.: "Performance of Petroleum Reservoirs Containing Vertical Fractures in the Matrix", *Soc. Pet. Eng. J.* (June, 1967) 221-228.
12. Chatas, A. T.: "Unsteady Spherical Flow in Petroleum Reservoirs", *Soc. Pet. Eng. J.* (June, 1966) 102-114, Eq. 2.
13. Chatas, A. T.: "A Practical Treatment of Nonsteady-State Flow Problems in Reservoir Systems", *Pet. Eng.* (May, June and Aug., 1953) 25.

14. Levorsen, A. J.: *Geology of Petroleum*, W. H. Freeman and Co., San Francisco (1954) 120.

15. Kazemi, H., Thomas, G. W. and Seth, M. S.: "The Interpretation of Interference Tests in Naturally Fractured Reservoirs", *Soc. Pet. Eng. J.* (Dec., 1969) 463-472.

APPENDIX A

SUMMARY OF POLLARD AND PIRSON-PIRSON FRACTURED RESERVOIR ANALYSIS

PRESSURE BUILDUP

$$\bar{p} - p_w(\Delta t) = C\, e^{-a_1 \Delta t} + D\, e^{-a_2 \Delta t} + (\bar{p} - p_{wf} - C - D)\, e^{-a_3 \Delta t} \quad \text{(A-1)}$$

$$PV_m = \frac{0.234\, qB}{2.3\, a_1 (C+D)\, c_m}, \text{ ft}^3 \quad \text{(A-2)}$$

$$PV_f = \frac{0.234\, qB}{2.3\, a_2\, D\, c_f}, \text{ ft}^3 \quad \text{(A-3)}$$

$$PV_s = \frac{0.234\, qB}{2.3\, a_3\, (\bar{p} - p_{wf} - C - D)\, c_s}, \text{ ft}^3 \quad \text{(A-4)}$$

The constants a_1, a_2, a_3, C and D may be obtained from the plot of data as shown schematically by Fig. 1. The first, second and third terms of the right-hand side of Eq. A-1 represent the decaying transients in the matrix, fracture and wellbore region, respectively.

APPENDIX B

WARREN AND ROOT FRACTURED RESERVOIR ANALYSIS[3]

PRESSURE DRAWDOWN IN INFINITE RESERVOIR

$$p_{wf}(t_D) = p_i - \frac{162.6\, q\mu B}{\bar{k} h_T} \left\{ \log t_D + .351 + .435\, Ei\,[-\lambda t_D/\omega(1-\omega)] - .435\, Ei\,[-\lambda t_D/(1-\omega)] + .87\, s \right\}. \quad \text{(B-1)}$$

PRESSURE BUILDUP IN INFINITE RESERVOIR

$$p_w(\Delta t_D) = p_i - \frac{162.6\, q\mu B}{\bar{k} h_T} \left\{ \log \frac{t_D + \Delta t_D}{\Delta t_D} - .435\, Ei\,[-\lambda \Delta t_D/\omega(1-\omega)] + .435\, Ei\,[-\lambda \Delta t_D/(1-\omega)] \right\}, \quad \text{(B-2)}$$

where

$$t_D = \frac{2.637 \times 10^{-4}\, \bar{k} t}{(\phi_1 c_1 + \phi_2 c_2)\, \mu\, r_w^2} \quad \text{(B-3)}$$

CALCULATION OF ω FROM BUILDUP CURVE

$$\omega = e^{-2.303\ (Dp/m)} = \frac{\phi_2 c_2}{\phi_1 c_1 + \phi_2 c_2} \quad \text{(B-4)}$$

MINIMUM TIME BEFORE QUASI-STEADY STATE BEGINS

Quasi-steady state in a spherical flow as well as in linear flow occurs at approximately t_{qss} hours as given by Chatas:[12,13]

$$t_{qss} = \frac{1}{2.637 \times 10^{-4}} \frac{\phi_1 c_1 \mu L^2}{2\, k_1} \quad \text{(B-5)}$$

Converting Eq. B-5 into dimensionless time by substituting Eq. B-5 in Eq. B-3, we get

$$(t_D)_{qss} = \frac{1}{2} \frac{\phi_1 c_1}{\phi_1 c_1 + \phi_2 c_2} L^2 \frac{\bar{k}}{k_1 r_w^2} \quad \text{(B-6a)}$$

or

$$(t_D)_{qss} = \frac{1}{2} (1-\omega) L^2 \frac{\bar{k}}{k_1 r_w^2} \quad \text{(B-6b)}$$

But $\lambda = \frac{\alpha k_1}{\bar{k}} r_w^2 = \frac{4n(n+2)}{\ell^2} \frac{k_1}{\bar{k}} r_w^2$ (see Ref. 3), (B-7)

where n = number of normal sets of fractures, 1, 2 or 3. ℓ is the characteristic dimension of the heterogeneous region.

From Eqs. B-6b and B-7, we can write

$$(t_D)_{qss} = \frac{1}{2} \frac{1-\omega}{\lambda} \left(\frac{L}{\ell} \right)^2 [4n(n+2)]. \quad \text{(B-8)}$$

If the dimensions of the parallelepiped are a, b and c, then[3]

$$\ell = \frac{3\, abc}{(ab + bc + ca)} \quad ; n = 3$$

$$\ell = \frac{2\, ab}{(a+b)} \quad ; n = 2 \quad \text{(B-9)}$$

$$\ell = a \quad ; n = 1$$

Notice that if $a = b = c$, then $\ell = a = b = c$. Let us assume that L in Eq. B-5 can be replaced by the smallest dimension of the building block. Then we can also show that $\ell \geq L$. Therefore $\ell = \gamma L$,

where $\gamma \geq 1$. Substituting in Eq. B-8 we get

$$(t_D)_{qss} = \frac{1}{2} \frac{1-\omega}{\lambda} \frac{4n(n+2)}{\gamma} \quad \ldots\ldots \text{(B-10)}$$

Let us now find the minimum of $(t_D)_{qss}$ while we hold ω and λ constant. Let $1 \leq \gamma \leq 100$ and $n = 1, 2, 3$. Thus,

$$(t_D)_{qss} = \epsilon \frac{1-\omega}{\lambda} \quad \ldots\ldots\ldots \text{(B-11a)}$$

where $.06 \leq \epsilon \leq 30$.

A reasonable ϵ will be larger than unity; however, we chose $\epsilon = 1$ for our discussion. Thus,

$$(t_D)_{qss} = \frac{1-\omega}{\lambda} \quad \ldots\ldots\ldots\ldots \text{(B-11b)}$$

From Fig. 5 of Ref. 3, the values of t_D^* (that is, the time where the first straight line disappears) were measured and then recorded in the upper half corner of each square in Table 4. The lower halves were filled with the values calculated from Eq. B-11b. By comparison of these entries, one notices that especially for practical cases where $\lambda < 10^{-6}$, the time before quasi-steady state begins is larger than the time of the disappearance of the early straight line. This implies either a paradox or inconsistency in Warren and Root's model. Nevertheless, we felt this was inconclusive and set out to study the problem further as shown in the main text.

CALCULATION OF EFFECTIVE FLOW CAPACITY

$$\bar{k}h = \frac{162.6\ q\mu B}{m} \quad \ldots\ldots\ldots \text{(B-12)}$$

TABLE 4 — VALUES OF t_D^*

λ \ ω	.001	.01	.1
5×10^{-9}	10^5 / $2. \times 10^8$	10^6 / $2. \times 10^8$	10^7 / 1.8×10^8
5×10^{-6}	10^2 / $2. \times 10^5$	10^3 / $2. \times 10^5$	10^4 / 1.8×10^5
5×10^{-3}	10^{-1} / $2. \times 10^2$	10^0 / $2. \times 10^2$	10^1 / 1.8×10^2

APPENDIX C

ADI PROCEDURE FOR SOLVING SYSTEMS 1 THROUGH 6

Referring to Fig. 4 and due to radial symmetry of flow equations, we have taken a pie-shaped slice of this basic structural unit of the reservoir and have covered it by a grid of mesh points (see Fig. 5). The wellbore axis is located in the apex.

First, we introduced the transformation $u = \ln(r/r_w)$ in the system of equations. The grid points were then chosen equidistant in the u-direction. This, of course, allows very close spacing of the mesh points around the wellbore where the pressure gradients are high.

We did not introduce any transformation for z-direction. However, we chose the first three rows (starting with the fracture) to be uniformly spaced. The remaining rows were spaced with gradually increasing mesh distances.

Secondly, notice that there is no flow across the top, the right-hand and the left-hand boundaries of the model, except at mesh point (1,1); that is, the fracture. Since the first row is the fracture axis, it is a plane of symmetry and a no-flow condition is in force. To represent the horizontal flow component at mesh point (1,1) by no-flow condition while the actual flow has been taken into account, we include an equivalent source term at (1,1) into the finite difference equation of Eq. 2. In fact, in the case where we wish the flow to occur into the wellbore at the entire mesh points of column one, we assume a no-flow condition on the left boundary and add proper source terms to Eq. 1.

Finally, a set of finite difference equations obtainable from Systems 1 through 6 is (recall that Φ is replaced by p):

u-DIRECTION

$$\left(r_w e^{(i-1)\Delta u}\right)^{-2} \frac{1}{(\Delta u)^2}\left[k_{i+\frac{1}{2},j}\left(p^{(k+1)}_{i+1,j,n+1} - p^{(k+1)}_{i,j,n+1}\right) - k_{i-\frac{1}{2},j}\left(p^{(k+1)}_{i,j,n+1} - p^{(k+1)}_{i-1,j,n+1}\right)\right] + \left[k_{i,j+\frac{1}{2}}\left(p^{(k)}_{i,j+1,n+1} - p^{(k)}_{i,j,n+1}\right)\Big/\Delta z_{j+\frac{1}{2}} - k_{i,j-\frac{1}{2}}\left(p^{(k)}_{i,j,n+1} - p^{(k)}_{i,j-1,n+1}\right)\Big/\Delta z_{j-\frac{1}{2}}\right]$$

$$+ \frac{2\, q_{i,j}\mu B}{2\pi r_w^2 \Delta z_j\, e^{(i-1)\Delta u}\left[e^{i\Delta u} - e^{(i-2)\Delta u}\right]} = \mu \phi_{i,j} c_{i,j} \frac{p^{(k+1)}_{i,j,n+1} - p_{i,j,n}}{\Delta t_{n+\frac{1}{2}}} \quad \ldots \text{(C-1)}$$

$I = 1, 2, \ldots, I;\ J = 2, 3, \ldots, J,\ n = 0, 1, 2, 3, \ldots;\ k = 0, 1, 2, \ldots K.$

$$\left(r_w e^{(i-1)\Delta u}\right)^{-2} \frac{1}{(\Delta u)^2}\left[k_{i+\frac{1}{2},1}\left(p^{(k+1)}_{i+1,1,n+1} - p^{(k+1)}_{i,1,n+1}\right) - k_{i-\frac{1}{2},1}\left(p^{(k+1)}_{i,1,n+1} - p^{(k+1)}_{i-1,1,n+1}\right)\right] + \frac{2k_{i,2}}{\Delta z_1}\left(p^{(k)}_{i,2,n+1} - p^{(k)}_{i,1,n+1}\right)\Big/(z_2 - z_1) + \frac{2q_{i,1}\mu B}{2\pi r_w^2 \Delta z_1 e^{(i-1)\Delta u}\left[e^{i\Delta u} - e^{(i-2)\Delta u}\right]} = \mu \phi_{i,1} c_{i,1} \frac{p^{(k+1)}_{i,1,n+1} - p_{i,1,n}}{\Delta t_{n+\frac{1}{2}}} \; ; \quad \ldots \quad \text{(C-2)}$$

$I = 1,2,\ldots,I;\ n = 0,2,3,\ldots;\ k = 0,1,2,\ldots,K.$

Another set of equations similar to Eqs. C-1 and C-2 must be written for the z-direction. This is done by replacing the iterative index (k) by ($k + 2$), while ($k + 1$) is fixed everywhere except on the right-hand sides of Eqs. C-1 and C-2, where $k + 1$ becomes $k + 2$.

To take the boundary conditions into account, we made use of mirror images at the boundaries. This is why we were interested in introducing a no-flow condition at all boundary mesh points. The initial condition (6) is also accounted for when $n = 0$.

In Eqs. C-1 and C-2 the following notations were used:

(a) $\Delta u = \frac{1}{I-1} \ln \frac{r_e}{r_w}$

(b) $\Delta z_j = (z_{j+1} - z_{j-1})/2$

(c) $\Delta z_{j+\frac{1}{2}} = z_{j+1} - z_j$

(d) $k_{i+\frac{1}{2},j} = 2\, k_{i+1,j}\, k_{i,j} / (k_{i+1,j} + k_{i,j})$

(e) $k_{i,j+\frac{1}{2}} = 2\, k_{i,j+1}\, k_{i,j} / (k_{i,j+1} + k_{i,j})$

(f) $\Delta t_{n+\frac{1}{2}} = t_{n+1} - t_n$

Also, the following points are worth noting.

(g) $q_{i,j} = 0$ for all i's and

$j = 2, \ldots, J$.

(h) $q_{1,1}$ = four times the flow rate at mesh point (1,1). The factor 4 is a reflection factor.

(i) $\Delta z_1 = \Delta z_{1+\frac{1}{2}} = \Delta z_{2+\frac{1}{2}} = \delta$. This particular choice was made for what follows in (j).

(j) If Eq. 2 is replaced by

$$\frac{1}{r}\frac{\partial}{\partial r}\left(k_f r \frac{\partial p}{\partial r}\right) + \frac{\partial}{\partial z}\left(k_f \frac{\partial p}{\partial z}\right) = \phi_f \mu c_f \frac{\partial p}{\partial t} \; ;$$

$$0 < z < \frac{\delta}{2}, \; r_w < r < r_e$$

and approximated by the usual three-point central difference formula, one notices that the result is equivalent to Eq. C-2, provided provision (i) is met. This simply implies that one can obtain identical results by solving Eq. C-1 by ADI procedure, provided the index, j, runs from 1 to J. The solution of such a system may be obtained as described in Ref. 9.

NOTES ON COMPUTING

Systems 1 through 7 are expressed in Darcy units (see Ref. 7, p. 16); when expressed in practical units, one must multiply the right-hand sides of Eqs. C-1 and C-2 by 3,800 and the source term by $141.2(2\pi)$. The sign of q is *negative* for production.

If practical field units are used, the first time step should be about 10^{-6} hours. The time step may be increased by a factor of 2 for every 10 time steps. The total number of iterations for each time step is about 2 to 4, provided a pressure tolerance of $\epsilon = 10^{-4}$ is used. The convergence criterion is

$$\left|\frac{p^{(k+2)}_{i,j,n+1} - p^{(k)}_{i,j,n+1}}{p_i - p^{(k+2)}_{i,j,n+1}}\right| \leq \epsilon \; .$$

We have provided for 25 × 21 mesh points on an IBM 360/65, using only core storage. However, we have used mostly 24 × 10 mesh points in some of our calculations. The total time for a complete pressure drawdown and buildup case is about 12 minutes (for drawdown alone, it is about 6 minutes). The material balance error is less than 3 percent, while flow rate error is less than 0.05 percent.

APPENDIX D

CALCULATION OF WARREN-ROOT CHARACTERIZATION PARAMETERS ω AND λ

Warren and Root[3] suggested that two parameters were sufficient to characterize the deviation of the behavior of a medium with double porosity from that of a homogeneous porous medium. One of the parameters ω was defined by Eq. D-1.

$$\omega = \frac{\phi_2 c_2}{\phi_1 c_1 + \phi_2 c_2} \quad \ldots \quad \text{(D-1)}$$

It is the ratio of the storage capacity of the secondary porosity (fracture) to the total storage capacity of the medium. The second parameter λ was defined by:

$$\lambda = \frac{\alpha \, k_1 \, r_w^2}{\bar{k}} \quad \ldots\ldots\ldots\ldots \text{(D-2)}$$

This dimensionless parameter governs the interporosity flow. Notice that α is a shape factor (has the dimension L^{-2}) and reflects the geometry of the matrix elements. For instance, it is equal to $12/b^2$ for the simplified structural model of this paper. Thus,

$$\lambda = 12 \frac{k_1}{\bar{k}} \left(\frac{r_w}{h}\right)^2 = 3 \frac{k_m}{\bar{k}} \left(\frac{r_w}{h/2}\right)^2 . \quad \text{(D-3)}$$

where

$$\bar{k} = \frac{k_f \delta + k_m (h-\delta)}{h} \quad \ldots\ldots\ldots \text{(D-4)}$$

Eq. D-1 may be written as Eq. D-5:

$$\omega = \frac{(PV_f/BV)\, c_f}{(PV_m/BV)\, c_m + (PV_f/BV)\, c_f} =$$

$$\frac{[\pi(r_e^2 - r_w^2)(\delta/2)]\, \phi_f c_f}{[\pi(r_e^2 - r_w^2)(h-\delta)/2]\, \phi_m c_m + [\pi(r_e^2 - r_w^2)(\delta/2)]\, \phi_f c_f}$$

or

$$\omega = \frac{\delta \, \phi_f c_f}{(h-\delta)\, \phi_m c_m + \delta \, \phi_f c_f} \quad \ldots\ldots \text{(D-5)}$$

Eqs. D-3 through D-5 will be used to calculate λ, $\bar{k}$ and ω, respectively. Average porosity $\bar{\phi}$ may be calculated from:

$$\bar{\phi} = \frac{\delta \, \phi_f + (h-\delta)\, \phi_m}{h} \quad \ldots\ldots\ldots \text{(D-6)}$$

The individual bulk porosities, ϕ_1 and ϕ_2, may be calculated in terms of point porosities, ϕ_m and ϕ_f, by Eqs. D-7 and D-8, respectively.

$$\phi_1 = \frac{(h-\delta)\, \phi_m}{h} \quad \ldots\ldots\ldots\ldots \text{(D-7)}$$

$$\phi_2 = \frac{\delta \, \phi_f}{h} \quad \ldots\ldots\ldots\ldots \text{(D-8)}$$

It is worthwhile to notice that ϕ_m and ϕ_f are point functions and represent local (or point) porosities, while ϕ_1 and ϕ_2 are bulk porosities for matrix and fracture, respectively.

★★★